Drop collision with a hot, dry solid substrate: Heat transfer during nucleate boiling

Jan Breitenbach, Ilia V. Roisman,* and Cameron Tropea
Institute for Fluid Mechanics and Aerodynamics, Technische Universität Darmstadt, Alarich-Weiss-Straße 10, 64287 Darmstadt, Germany
(Received 27 October 2016; published 7 July 2017)

Outcomes from an isothermal drop impact onto a surface (rebound, deposition, or splash) are determined by the impact parameters, liquid material properties, substrate morphology, and wettability. Drop impact onto a hot surface can be accompanied by Marangoni effects, nucleate or film boiling, and evaporation. The main focus of this experimental study is the characterization of the hydrodynamic outcome of a single-drop impact onto a hot surface. Drop impact phenomena have been observed and characterized using a high-speed video system. The impact parameters of the drop and the surface temperature have been varied. The observations lead to a classification of impact outcomes into several regimes: evaporation, nucleate boiling, foaming, transitional boiling, and film boiling. The contact time of the impinging droplet on the surface has been measured, and a model for this time and for the heat flux from the substrate to the drop has been proposed for the nucleate boiling regime. Comparison of model predictions to existing literature data is good.

DOI: 10.1103/PhysRevFluids.2.074301

I. INTRODUCTION

The phenomena of drop impact onto hot surfaces have been extensively investigated in the past; however, many questions and dependencies remain unclear. For a pure isothermal drop impact the outcome depends mainly on the parameters: impact velocity, substrate morphology and wettability, and liquid properties [1]. Comprehensive reviews of these phenomena can be found in Refs. [2] and [3]. However, the phenomena of drop impact onto hot surfaces can be considerably more complicated, involving Marangoni effects, liquid boiling, evaporation, and changes of temperature-dependent material properties. Hence, the outcome of a drop impact onto a substrate can be significantly influenced by the substrate temperature. At high surface temperatures, higher than the Leidenfrost point [4], a vapor layer between the droplet and the surface prevents direct contact between the liquid drop and the surface [5–9]. The Leidenfrost point is influenced by the surface roughness [10], surface structure [11,12] and liquid rheological or interfacial properties [13–15]. For example, it has been recently shown [16] that substrates coated by nanofiber mats can completely prevent film boiling of a sessile drop. Besides the film boiling regime (above the Leidenfrost point), the bubble (or nucleate) boiling, transitional boiling, and single-phase drop deposition are also identified as possible outcomes of drop impact onto hot surfaces [17–20]. Moreover, the substrate temperature also effects the splashing threshold and the characteristic size of secondary droplets [21,22].

Drop impact is often studied in relation to spray cooling [23], since this is a promising technology for cooling of devices with very high heat flux densities. The main measure of the effectiveness of spray cooling is the achieved heat flux density [24–26] as a function of the operating thermodynamic regimes and the substrate structure [27,28] and the critical heat flux [29,30]. Correlations for these important quantities are mainly empirical in nature, since the hydrodynamics and thermodynamics of the cooling process with interacting drops and sprays are complicated and not yet completely understood.

*roisman@sla.tu-darmstadt.de

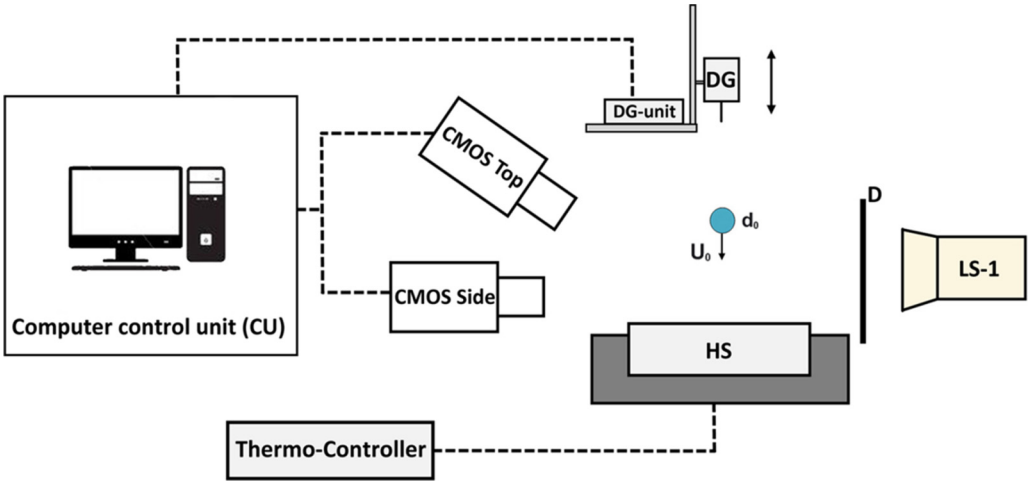

FIG. 1. Experimental setup: heating system (HS) with controller, drop generation unit (DG), illumination system (LS-1) with a diffuser plate (D), CMOS high-speed cameras (CMOS Side and Top), and a computer for control and data acquisition (CU).

The main focus of the present study is the dynamics of drop impact onto a hot surface for different hydrodynamic and thermodynamic conditions. Drop impact, spreading, rebound, breakup, or evaporation on a hot substrate are observed using a high-speed video system. The heat transfer in the solid substrate under the sessile drop is analyzed theoretically. This analysis allows prediction of the amount of heat transferred to the drop and estimation of the typical time of drop evaporation, two quantities of paramount importance for spray cooling applications. The model agrees very well with the experimental data.

II. EXPERIMENTAL METHOD

A. Experimental setup

The experimental setup is shown schematically in Fig. 1 and comprises a heating system (HS), the drop generation (DG), the illumination system (LS-1), CMOS high-speed cameras (CMOS Side and Top), and a computer for control and data acquisition (CU).

A detailed sectional view of the impact target (HS) is shown in Fig. 2. The impact surface is a polished aluminum cylinder (EN AW 7075) with a diameter of 50.8 mm, embedded in a heated copper cylinder. To ensure a high-quality surface, the aluminum was polished in several stages with increasing grades of sandpaper and polishing paste (Micro Mesh 1500–12 000 grit), reaching a final surface roughness of $R_a \approx 0.1$ μm. Subsequently, the heater was cleaned with isopropyl alcohol to remove polish residues. To heat the impact surface a 250 W cartridge heater (hotset hotrod HHP) mounted in the heating cylinder is used, and ceramic with a low thermal conductivity is used to insulate the sidewalls of the cylinder. A Type-K thermocouple with a diameter of 1 mm is placed 0.5 mm below the impact point in the aluminum surface. Prior to drop impact, the temperature difference between the thermocouple and the surface is neglected. Using a controller (hotset c448), the initial surface temperature can be varied between $T_0 = 50$ and 400 °C. The drop is generated with a blunt hydrophobic needle (outer diameter D_N) supplied with water by a piezoelectric micropump until the drop detaches due to its own weight. Double-distilled water (density $\rho_w = 998\,\mathrm{kg/m^3}$, viscosity $\nu_w = 10^{-6}\,\mathrm{m^2/s}$, surface tension $\sigma_w = 72.75 \times 10^{-3}\,\mathrm{N/m}$, liquid temperature $T_l = 20\,^\circ\mathrm{C}$) is used as fluid. The size of the needle has been chosen as gauge 27 with an outer diameter $D_N = 0.4$ mm to generate a drop diameter of $d_0 = 2.15$ mm. By changing the height H_0 of the drop

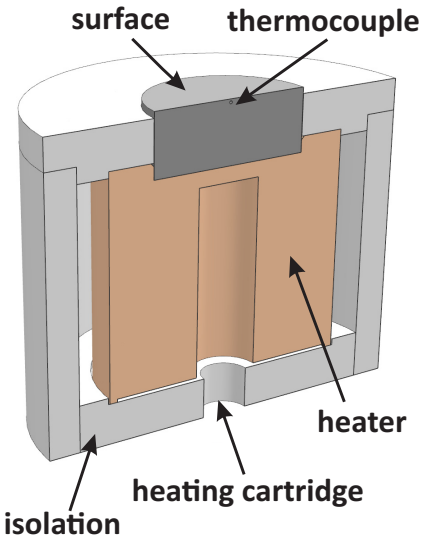

FIG. 2. Impact target comprising an aluminum cylinder on top of a copper heater, heated by a 250 W cartridge heater and insulated by a ceramic enclosure. A thermocouple is placed 0.5 mm below the impact point on the surface.

generator, different impact velocities $v_0 = 0.3$–3.0 m/s can be produced. For each impact the drop diameter and drop velocity are calculated by image postprocessing.

To record both side view and top view of the drop impact, two synchronous CMOS high-speed cameras (2 × Phantom V12.1) with a maximum resolution of 1280 × 800 pixel at 6242 frames/s are used. Both high-speed cameras have been equipped with a 60 mm microlens (Nikon AF NIKKOR 1:2.8 D) and spacer rings (Nikon). With this apparatus a spatial resolution of 84 pixels/mm for the side view and 60 pixels/mm for the top view has been achieved. The illumination system (LS-1) is a 120 W LED spotlight (Constellation 120 E) and is placed behind the drop to yield shadowgraphy imaging. To achieve a more uniform illumination a 3 mm optical diffuser plate (D) is placed between the LED spotlight and the drop impact. Postprocessing of the images and the measurement of the contact time is performed with MATLAB and Vision Research PCC.

B. Observations of drop impact phenomena

Figure 3 pictures various microscopic thermodynamic phenomena observed in the experiments: evaporation (a), nucleate boiling (b), foaming (c), transition boiling (d), and film boiling (e). The same phenomena have been observed before [17]. During evaporation, few or no bubbles can be observed inside the drop; therefore the drop vaporizes relatively slowly. This behavior is observed

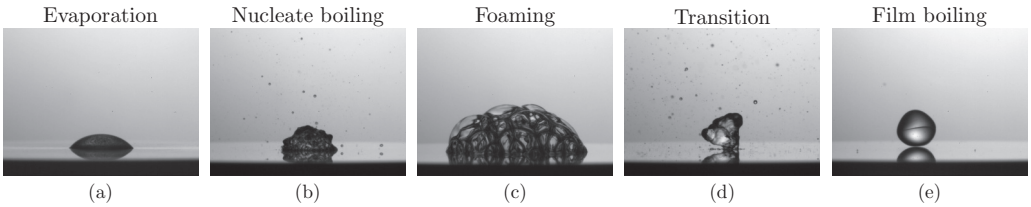

FIG. 3. Microscopic thermodynamic boiling phenomena: evaporation (a), nucleate boiling (b), foaming (c), transition (d), and film boiling (e).

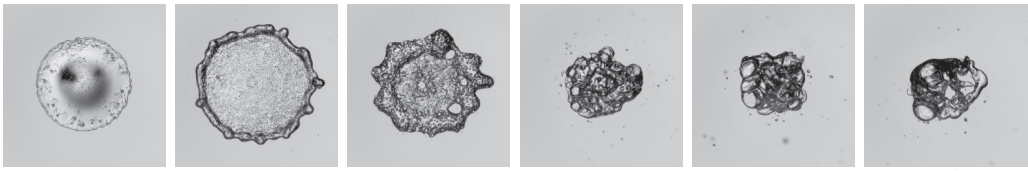

FIG. 4. Exemplary bottom view through a transparent sapphire substrate on a water drop during nucleate boiling ($T_0 = 160\,^\circ$C). Note that sapphire is used as impact target, and the temperature threshold for nucleate boiling can be different from the aluminium substrate.

at low surface temperatures $\Delta T_S = T_0 - T_{\mathrm{sat}} \lesssim 15\,^\circ$C above the saturation temperature T_{sat}. It should be noted that the temperature thresholds for the various phenomena are determined for an aluminum surface. For further surface materials, e.g. sapphire substrate, the thresholds could be slightly different, since they additionally depend on the substrate material properties.

At higher surface temperatures, $\Delta T_S \gtrsim 15\,^\circ$C, drop evaporation is caused mainly by nucleate boiling. With nucleate boiling small vapor bubbles frequently form at the drop-wall surface, detach from the surface, ascend through the drop, and possibly coalesce with other bubbles. When the bubbles break through the liquid-gas interface they collapse, and fine secondary droplets are produced.

In the foaming phenomena the vapor bubbles grow much larger; no coalescence and no separation from the liquid-gas interface are observed. In this subcategory of nucleate boiling, the entire drop starts to foam. This phenomenon is yet not fully understood [31]. An explanation is that small amounts of dissolved ionic salt in the double-distilled water prevent bubble coalescence due to electrostatic effects and changes of surface tension. The influence of the dissolved ionic salt on boiling water drops was shown in Ref. [32]. The presence of electrical charge on the bubble surface due to ionic salts produces a repulsive force, preventing the bubbles from approaching each other [33]. Some theories also claim that during boiling the dissolved salt cannot diffuse quickly enough and the local salt concentration in the thinning liquid layer increases; therefore the surface tension increases, the coalescence of the bubbles is delayed, and the water drop foams [34].

Transition boiling is a transient phenomena between nucleate boiling and film boiling. It is observed for surface temperatures higher than $\Delta T_S \gtrsim 50\,^\circ$C. The vapor bubble generation rate rises quickly, caused by the high wall temperature. Consequently, bubbles coalesce and form a vapor layer over some portions of the area between the drop and the surface, while the rest of the drop wets the surface. The transition regime is very unstable, and liquid layers frequently collapse. The drop appears to be dancing on the surface. Moreover, secondary droplets are generated.

By increasing the surface temperature beyond the Leidenfrost point the heat flux transferred to the water drop reduces [4], since the water vapor is ineffective for heat conduction. After reaching the Leidenfrost temperature T_{Leid}, film boiling occurs. At this condition the substrate surface is covered with a vapor layer and the drop does not wet the surface anywhere; heat flux and friction between the drop and the surface decrease. As a consequence, the drop lifetime increases significantly.

A bottom view through a transparent target on a drop in the nucleate boiling regime is shown in Fig. 4 and as a video in the Supplemental Material [35]. In this typical example, after 9 ms (which is much shorter than the overall time of drop contact with the wall, which is of the order of seconds), the wetted area of the drop is already completely covered by vapor bubbles. This phenomenon is caused by the well-known fact that drop impact initiates creation of numerous microbubbles [36–39], which lead to further bubble nucleation.

After impact onto a solid substrate the drop first spreads and then starts to recede. The duration of drop spreading and receding is approximately of the order d_0/v_0, which in the present case is approximately 5 ms. At longer times the wetted area doesn't change significantly despite the mass reduction of the drop, caused by an intensive evaporation and creation of secondary drops (see the

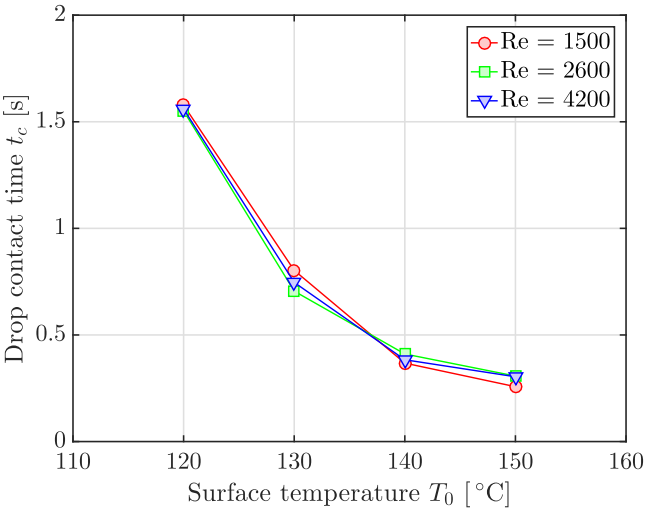

FIG. 5. Contact times in the nucleate boiling regime for various initial wall temperatures and impact parameters.

images of the wetted spot in Fig. 4 for times larger than 6 ms). In the nucleate boiling regime the contact line remains pinned almost until complete drop evaporation for all the observed cases. This is an interesting observation. The contact line pinning is explained by the continuous generation of the bubbles, which prevents the receding of the contact line.

During nucleate boiling some drop mass is lost due to the generation of small secondary drops. The mass of the secondary drops is significant in the transition boiling regime, when the drop rebound is significant. In the nucleation boiling regime considered in this study, the total mass of the secondary drops usually does not exceed 10% of the initial drop mass. Therefore, the assumption can be made that in the nucleate boiling regime most of the heat from the substrate goes into drop vaporization through intensive bubble creation.

C. Contact time of an impacting drop in the nucleate boiling regime

The duration of contact between the drop and the hot substrate, the contact time, is an important quantity which strongly influences the heat removed by the impacting drop from the substrate. As such, this quantity is a necessary element of any spray cooling model. In Fig. 5 an example contact time in the nucleate boiling regime is shown as a function of the initial surface temperature T_0. This time is measured until complete drop evaporation on the substrate. Figure 6 shows an impinging drop onto a aluminum substrate in the nucleate boiling regime at initial surface temperatures $T_0 = 140\,^{\circ}\mathrm{C}$. The cases of drop rebound are not shown in this graph and are not considered in this study. In the nucleate boiling regime the contact time reduces with increasing initial surface temperature. The

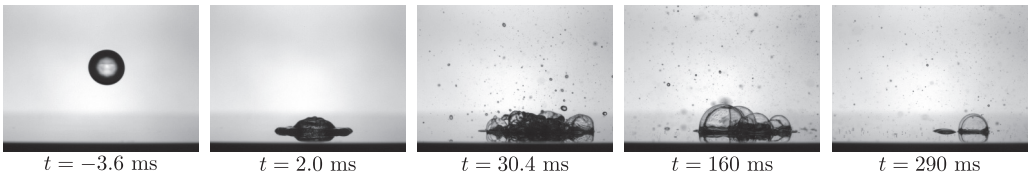

FIG. 6. Impinging water droplet in the nucleate boiling regime at initial surface temperatures $T_0 = 140\,^{\circ}\mathrm{C}$ for the impact parameters $d_0 = 2.15$ mm, $v_0 = 0.7$ m/s, Reynolds number Re = 1500.

contact time in the nucleate boiling regime is not influenced by the impact parameters (Fig. 5). The dependence of the contact time t_c on the initial substrate temperature is expressed well by the relation

$$t_c \sim (T_0 - T_{\mathrm{sat}})^{-1.92}, \tag{1}$$

obtained by fitting of the experimental data.

Existing models for the heat transfer during boiling [40–44] are not applicable for the description of the phenomena considered in our study. An approximate model for nucleate boiling which accounts for only main physical influencing factors and is able to predict the evaporation time of a drop in the nucleate boiling regime will be described in the next section.

III. EVALUATION OF HEAT TRANSFER IN THE NUCLEATE BOILING REGIME

A. Heat transfer during the waiting time

During a very short time interval after drop collision the bubbles created by the drop impact are very small. Their size is comparable with the roughness of the substrate, which is of the order of 1 μm. The relative area of the wetted substrate occupied by bubbles is initially very small. In our experiments, shown in Fig. 4, the waiting time for bubble nucleation is approximately 1 ms and the typical time for complete saturation of the wetted area by bubbles is 3 ms.

At the initial phase of drop spreading the temperature at the solid-liquid interface, called the contact temperature, can be estimated considering the heat conduction in the substrate, heat convection in the spreading drop, and the boundary conditions at the interfaces. In the absence of evaporation these boundary conditions are described by the continuity of the temperature and of the heat flux in the solid and liquid regions at the interface. The heat conduction in the solid substrate occurs in a thermal boundary layer of thickness $h_w \sim \sqrt{\alpha_w t}$, where α_w is the thermal diffusivity of the substrate material. In the liquid region the problem is determined by the viscous boundary layer of thickness $h_{\nu l} \sim \sqrt{\nu_l t}$ and the thermal boundary layer of thickness $h_l \sim \sqrt{\alpha_l t}$, which is influenced by the flow in the spreading drop. Here ν_l and α_l are the kinematic viscosity and thermal diffusivity of the liquid drop material, respectively. An exact solution of this problem can be found in Ref. [45]. The expressions for the contact temperature and for the heat flux density at the interface are obtained in the form

$$T_c = \frac{\mathscr{I}(\mathrm{Pr}_l) e_w T_0 + e_l T_l}{\mathscr{I}(\mathrm{Pr}_l) e_w + e_l}, \tag{2}$$

$$\dot{q} = \frac{e_l e_w (T_0 - T_l)}{[e_l + \mathscr{I}(\mathrm{Pr}_l) e_w] \sqrt{\pi} \sqrt{t}}, \tag{3}$$

where T_l and T_0 are the initial temperatures of the drop and of the substrate, Pr_l is the Prandtl number for the drop liquid, $e_l \equiv \lambda_l / \alpha_l^{1/2}$ and $e_w \equiv \lambda_w / \alpha_w^{1/2}$ are the corresponding thermal effusivities of the liquid and the solid substrate, and λ_l and λ_w are their thermal conductivities, respectively.

Function $\mathscr{I}(\mathrm{Pr}_l)$ of the Prandtl number can be approximated by fitting the solution in [45] by a power function

$$\mathscr{I}(\mathrm{Pr}_l) \approx 0.17 + 0.47 \mathrm{Pr}_l^{0.1}, \quad \mathrm{Pr}_l < 100. \tag{4}$$

It can be shown that in the limit $\mathrm{Pr}_l \to \infty$ the value of $\mathscr{I}(\mathrm{Pr}_l)$ approaches unity, and the expression for the contact temperature is reduced to the well-known form for the contact temperature of the two solid semi-infinite bodies [46]:

$$T_c = \frac{e_w T_0 + e_l T_l}{e_w + e_l}, \tag{5}$$

$$\dot{q} = \frac{e_l e_w (T_0 - T_l)}{(e_l + e_w) \sqrt{\pi} \sqrt{t}}. \tag{6}$$

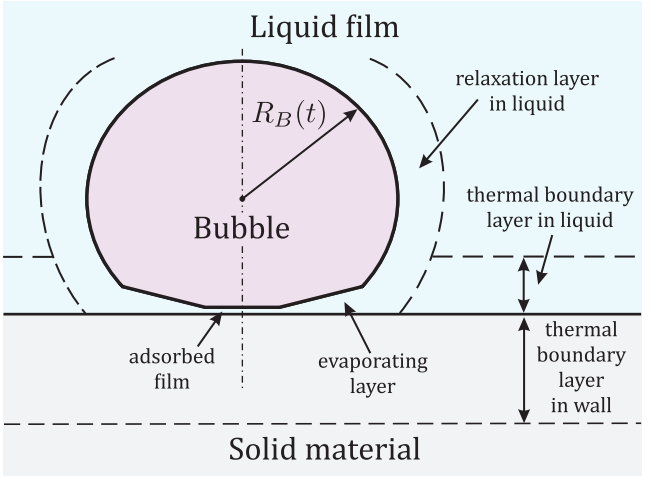

FIG. 7. Sketch of a heated wall with vapor bubble and surrounding liquid.

Solution (2)–(3) has recently been validated by comparison with the numerical simulations [47]. The agreement is rather good. However, during nucleate boiling the waiting time for the inception of the bubble growth is three orders of magnitude smaller than the drop evaporation time. The solution (2)–(3) therefore has no significant influence on the final expression for the evaporation time.

B. Single bubble formation

Heterogeneous nucleation and bubble growth, associated with the pool boiling regime, has been studied rather extensively. Two main regimes of the bubble growth are considered: inertia-dominated growth and heat-transfer-controlled growth [44]. The bubble radius, after some waiting period, expands as the square root of time

$$R_B = \beta t^{1/2}, \tag{7}$$

where factor β is determined by the thermodynamic material properties and the initial temperatures of the substrate and the liquid.

In many existing theoretical solutions for the bubble growth [48–50], the temperature of the wall interface exposed to the bubble is assumed to be close to the saturation temperature T_{sat}. The reason for this is in the existence of a thin evaporating liquid film on the wall. The existence of this wall film is the only possible explanation of the fact that the bubble reaches sizes much larger than the thermal boundary layer (the majority of the bubble surface is therefore located in the relatively cold region of the drop). This liquid film beneath the bubble is formed by a process similar to dip coating [51,52] and is usually referred to as evaporation microlayer. The wall temperature under the bubble only slightly exceeds the saturation temperature, since the liquid film thickness is rather small. Outside the bubble, near the interface, a relaxation microlayer is usually considered. A sketch of the vapor bubble with surrounding liquid on the heated wall is schematically shown in Fig. 7.

The thickness of the evaporating layer [52] is determined by the thickness of the laminar boundary layer

$$\delta_{l0} = 3.012\left(\frac{\nu_l}{\beta^2}\right)\text{Pr}_l^{-1/3} R_B. \tag{8}$$

As soon as the wall film evaporates, temperature fluctuations are possible, which also immediately influence the evolution of the bubble radius. At this stage a thin adsorbed film beneath the bubble is assumed in Ref. [53], and the evaporation occurs mainly in the micro-region of an advancing contact

line. In this case the boundary condition at the interface beneath the bubble is the vanishing of the heat flux in the area beneath the bubble.

In the model [43] the existence of the evaporating microlayer is completely neglected, and the contact temperature is determined from the one-dimensional solution (5)–(6), associated with the contact of two solid semi-infinite bodies.

In the present experiments the characteristic size of the bubbles in the drop are of order of 1 mm already after 10 ms. At this time the thickness of the thermal boundary layer in the liquid $\sqrt{\alpha_l t}$ is approximately 40 μm. The bubble size is much larger than the thickness of the thermal boundary layer. Therefore, bubble evaporation occurs only in the region in the close vicinity of the wall, near the contact line and in a thin wall film. This means that the bubble growth is caused solely by the evaporation in the evaporating microlayer. This conclusion is supported by the fact that the predictions of the drop evaporation time based on the models [43,53] do not agree well with the experimental data.

The value of the factor in the expression for the radius of the bubble (7) is $\beta \sim 10^{-3}\,\mathrm{m/s^{0.5}}$, which is estimated by fitting the radius evolution of the observed bubbles. Therefore, the estimated thickness of the evaporating layer is $\delta_{l0} \sim 10^{-2} R_B$. For the heat flux density $\dot{q} \sim 10^6\ \mathrm{W\ m^{-1}\ K^{-1}}$, estimated in this study (see Fig. 12), and the average bubble radius 0.5 mm, for which $\delta_{l0} \approx 4\,\mu$m, the temperature at the interface is approximately 7 K. A static microlayer of the thickness δ_{l0} at this heat flux evaporates in approximately 10 ms. This time is comparable with the observed bubble growth time before its departure or collapse. Therefore, the evaporating layer exists during the entire process of bubble growth.

C. Nucleate boiling in an impacting drop

Drop collision with the hot substrate initiates the start of heat transfer in the solid and liquid regions. In the solid wall, heat is transferred by conduction. In the liquid region, heat conduction is determined by the rather complicated flow in the drop during its spreading, influenced by the expansion and motion of the vapor bubbles.

The overall energy balance of heat transfer from the evaporating sessile drop and the heat flux from the substrate is given by

$$\int_0^{t_c} A_c(t)\dot{q}(t)\,dt \approx \rho_l L^* \frac{\pi d_0^3}{6}, \tag{9}$$

where A_c is the contact area, $\dot{q}$ is the heat flux density at the solid-liquid interface, d_0 is the initial drop diameter, ρ_l is the density of the liquid, and $L^* = L + \Delta H_0$ is the sum of the latent heat of evaporation L and the enthalpy difference ΔH_0 between the initial drop and saturated liquid. Equation (9) is based on the assumption that the energy goes entirely into drop evaporation. This assumption is valid only for the cases of nucleate boiling, for which the relative mass of fine secondary droplets, generated during drop boiling, is small. In the absence of drop rebound the ejected mass ratio in the nucleate boiling regime, estimated in our experiments, is less than 10%.

At the first instant of drop contact a thermal boundary layer develops in the substrate. The thickness of the thermal boundary layer is $h_w \sim \sqrt{\alpha_w t}$, where α_w is the thermal diffusivity of the wall material. Since the thickness of the boundary layer is much smaller than the drop diameter, the heat conduction in the substrate can be approximated by a one-dimensional model. The temperature at the solid-liquid interface is not uniform. It is influenced by the appearance and growth of the bubbles initiated by heterogeneous nucleation at the substrate surface. As mentioned in the Sec. III A, the temperature of the wall beneath the bubble and at the substrate in the relaxation layer outside the bubble is close to the saturation temperature T_{sat}, since it is determined by the liquid evaporation in the thin evaporation microlayer.

Moreover, as seen in the exemplary bottom view of the boiling drop in Fig. 4, the relative area of the bubbles on the substrate during the long phase of drop evaporation (at times larger than the

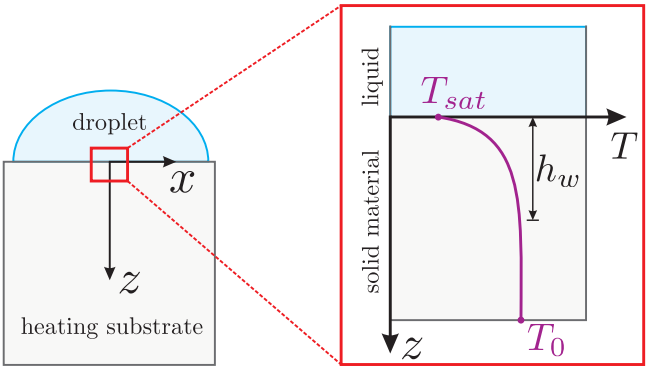

FIG. 8. Sketch of the assumed temperature distribution within the solid material due to contact of the liquid with the substrate. The solid-liquid interface is located at $z = 0$.

time of drop spreading, 9 ms) is rather high, above 90%. Therefore, as a rough approximation we can assume a nearly uniform interface temperature $T_{\rm sat}$ of the substrate.

The geometry and the definition of the coordinate system are shown schematically in Fig. 8. At $t = 0$ the liquid is placed in contact with a semi-infinite wall $z > 0$ at the initial temperature T_0. The heat conduction equation in the wall

$$\frac{\partial T_w}{\partial t} - \alpha_w \frac{\partial^2 T_w}{\partial z^2} = 0, \tag{10}$$

has to be solved subject to the boundary conditions

$$T_w = T_{\rm sat} \quad \text{at} \quad z = 0; \quad T_w \to T_0 \quad \text{at} \quad z \to \infty, \tag{11}$$

where $T_w(z,t)$ is the temperature in the wall region. The similarity solution of Eqs. (10)–(11) is well known [45]:

$$T_w(z,t) = T_{\rm sat} + (T_0 - T_{\rm sat})\,\mathrm{erf}\left(\frac{z}{2\sqrt{\alpha_w t}}\right). \tag{12}$$

The heat flux density at the solid-liquid interface can be expressed with the help of Eq. (12) as

$$\dot{q}(t) \equiv \lambda_w \frac{\partial T_w}{\partial z}\bigg|_{z=0} = \frac{e_w \Delta T_w}{\sqrt{\pi}\sqrt{t}}, \tag{13}$$

where λ_w is the thermal conductivity of the wall material, e_w is the thermal effusivity $e_w = \sqrt{\lambda_w \rho_w c_p}$, and $\Delta T_w = T_0 - T_{\rm sat}$ is the overall temperature difference in the wall (see Fig. 8).

The contact area $A_c(t)$ changes during drop spreading and receding. However, since the contact time t_c in the nucleate boiling regime is much longer than the observed impact time ($t_{\rm imp} \sim d_0/v_0$, where v_0 is the impact velocity), the contact area can be estimated in the form

$$A_c \approx k_{\rm w} \pi d_0^2, \tag{14}$$

where the coefficient $k_{\rm w}$ is determined primarily by the surface structure and wettability. The coefficient $k_{\rm w}$ accounts also for the effective drop growth due to bubble expansion, for the mass loss during atomization, and for some small deviation of the interface temperature from the saturation temperature. This coefficient is of order unity and can be determined from the experiments in Fig. 5(a). Substituting expressions (12), (13), and (14) in the energy balance equation (9) yields

$$t_c = \pi \left(\frac{\rho_l L^* d_0}{12 k_{\rm w}\, e_w \Delta T_w}\right)^2. \tag{15}$$

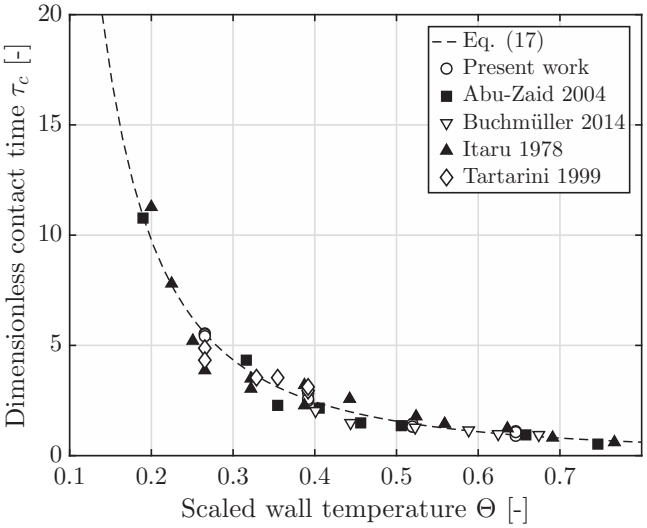

FIG. 9. Dimensionless contact time of a water drop from this study and existing literature data [54–57] as a function of the scaled wall temperature Θ, in comparison with the theoretical prediction [Eq. (17)]. The initial drop diameter in the experiments ranges from 2.1 to 4.6 mm, and the wall materials are polished aluminum, carbon steel, and stainless steel.

It is important to note that the obtained dependence $t_c \sim \Delta T_w^{-2}$ is in good agreement with the empirical correlation (1). Introducing the scaled wall temperature and dimensionless time in the form

$$\Theta = \frac{T_0 - T_{\rm sat}}{T_{\rm sat} - T_l}, \quad \tau = \frac{t}{\pi}\left[\frac{12\, e_w\,(T_{\rm sat} - T_l)}{\rho_l L^* d_0}\right]^2 \tag{16}$$

allows the contact time to be given in dimensionless form:

$$\tau_c = \frac{1}{k_{\rm w}^2\,\Theta^2}. \tag{17}$$

The contact times from this study and those found in literature from Abu-Zaid [54], Buchmüller [55], Itaru and Kunihide [56], and Tartarini *et al.* [57] are compared with the theoretical prediction [Eq. (17)] in Figs. 9 and 10. The agreement is good for all the cases. For the data shown in Fig. 9 (for the normal pressure conditions) the coefficient $k_{\rm w} = 1.6$ is determined by fitting to the experimental data. This parameter is the same for all the substrates used in the experiments, since their wettability properties are similar [58]. The observed contact angle is approximately 90°. At this angle the estimated value of the coefficient $k_{\rm w} = 2^{2/3} \approx 1.58$ is very close to the value obtained from the experiments.

At the elevated pressure conditions shown in Fig. 10 the best fit to the experimental data from Ref. [55] yields $k_{\rm w} = 1.0$. Some difference between the values of $k_{\rm w}$ can be caused by the conditions at the target surface (some sediments have been observed in the experiments [55]) and by the increase of the contact angle with the ambient pressure [59], leading to the decrease of the contact area of the drop. The corresponding dimensional contact times for the elevated pressure conditions are additionally shown in Fig. 11 as a function of the overheated wall temperature $\Delta T_w = T_0 - T_{\rm sat}$ for the same initial drop diameter.

With Eqs. (13) and (15) the time-averaged heat flux of the drop evaporation can be expressed as

$$\langle \dot{q} \rangle_c = \frac{24 k_{\rm w}\, e_w^2\, \Delta T_w^2}{\rho_l \pi\, L^* d_0}. \tag{18}$$

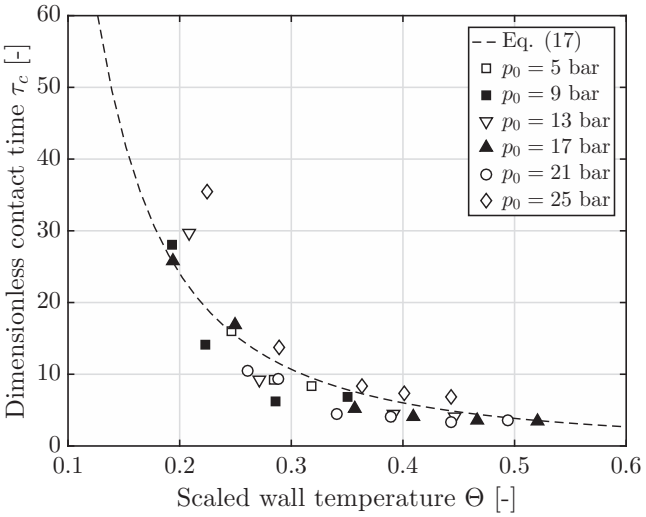

FIG. 10. Dimensionless contact time of a water drop on aluminum surface at various ambient pressures [55] as a function of the scaled wall temperature Θ, in comparison with the theoretical predictions [Eq. (17)]. The ambient pressure ranges from 5 to 25 bar.

Figure 12 shows the estimated time averaged heat flux for different surface temperatures and impact parameters. This value is important for the development of a spray cooling model in the nucleate boiling regime. In Fig. 12 the averaged heat flux is estimated as $\langle \dot{q} \rangle_c = 1/t_c \int_0^{t_c} \dot{q}\, dt$, where $\dot{q}$ is defined in (13), and the contact time t_c is measured in the experiments for different impact Reynolds numbers and surface temperatures. Additionally the theoretical predictions (18) are shown to extend the range of the surface temperatures from 110 to 160 °C.

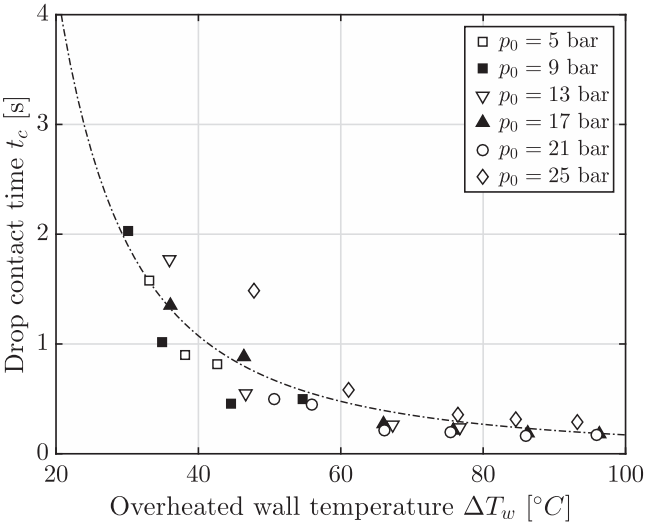

FIG. 11. Contact time of a water drop on a aluminum surface at various ambient pressures [55] as a function of the overheated wall temperature ΔT_w for the same initial drop diameter. The ambient pressure ranges from 5 to 25 bar.

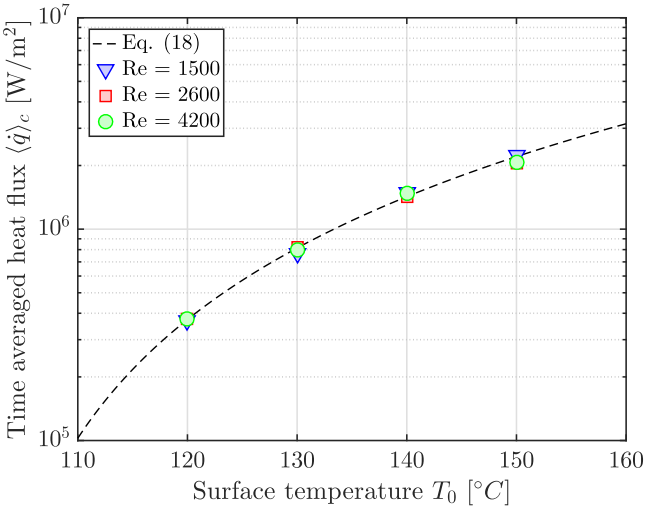

FIG. 12. Time-averaged heat flux for different impact parameters, calculated using the measured contact times. The theoretical prediction (18) is also shown for the substrate temperature range from 110 to 160 °C.

For the drop diameter used in the experiments, the average heat flux is in the range from 10^5 to 2×10^6 W/m^2. In many cases these values are much larger than heat flux densities achieved by steady sprays [29,60], because intensive sprays create a continuous water film, which reduces the heat flux density significantly. The optimal spray for cooling purposes can be envisioned for the condition that all the impacting drops have just enough time to evaporate on the wall before the next drop arrives, i.e., all drops impact onto a dry substrate. This means that the wetted surface ratio, $\pi d_0^2 t_c \dot{N} < 1$, has to be of order unity. Here $\dot{N}$ is the spray number density. The optimum mass flux density of the spray can thus be estimated from

$$\dot{m} \approx \frac{\rho_l d_0}{t_c}. \tag{19}$$

The optimum mass flux density $\dot{m}$ of spray can be determined using the expression (17) for the contact temperature in the nucleate boiling regime. However, practically, such optimal sprays can be applied only over a finite temperature range, since the contact time t_c depends on the substrate temperature.

ACKNOWLEDGMENT

This research was supported by the German Research Foundation (Deutsche Forschungsgemeinschaft) in the framework of the SFB-TRR 75 Collaborative Research Center, Subproject C4.

[1] R. Rioboo, C. Tropea, and M. Marengo, Outcomes from a drop impact on solid surfaces, Atom. Sprays **11**, 155 (2001).

[2] A. L. Yarin, Drop impact dynamics: Splashing, spreading, receding, bouncing, Annu. Rev. Fluid Mech. **38**, 159 (2006).

[3] M. Marengo, C. Antonini, I. V. Roisman, and C. Tropea, Drop collisions with simple and complex surfaces, Curr. Opin. Colloid Interface Sci. **16**, 292 (2011).

[4] J. G. Leidenfrost, On the fixation of water in diverse fire, Int. J. Heat Mass Transfer **9**, 1153 (1966).

[5] D. Quéré, Leidenfrost dynamics, Annu. Rev. Fluid Mech. **45**, 197 (2013).
[6] T. Tran, H. J. J. Staat, A. Prosperetti, C. Sun, and D. Lohse, Drop Impact On Superheated Surfaces, Phys. Rev. Lett. **108**, 036101 (2012).
[7] N. Z. Mehdizadeh and S. Chandra, Boiling during high-velocity impact of water droplets on a hot stainless steel surface, Proc. R. Soc. London Ser. A **462**, 3115 (2006).
[8] M. Pasandideh-Fard, S. D. Aziz, S. Chandra, and J. Mostaghimi, Cooling effectiveness of a water drop impinging on a hot surface, Int. J. Heat Fluid Flow **22**, 201 (2001).
[9] J. D. Bernardin and I. Mudawar, The Leidenfrost point: Experimental study and assessment of existing models, ASME J. Heat Transfer **121**, 894 (1999).
[10] J. Bernardin, C. J. Stebbins, and I. Mudawar, Effects of surface roughness on water droplet impact history and heat transfer regimes, Int. J. Heat Mass Transfer **40**, 73 (1996).
[11] D. Arnaldo del Cerro, Á. G. Marín, G. R. B. E. Römer, B. Pathiraj, D. Lohse, and A. J. Huis in 't Veld, Leidenfrost point reduction on micropatterned metallic surfaces, Langmuir **28**, 15106 (2012).
[12] H. Nair, H. J. J. Staat, T. Tran, A. van Houselt, A. Prosperetti, D. Lohse, and C. Sun, The Leidenfrost temperature increase for impacting droplets on carbon-nanofiber surfaces, Soft Matter **10**, 2102 (2014).
[13] V. Bertola, An experimental study of bouncing Leidenfrost drops: Comparison between newtonian and viscoelastic liquids, Int. J. Heat Mass Transfer **52**, 1786 (2009).
[14] V. Bertola, Drop impact on a hot surface: Effect of a polymer additive, Exp. Fluids **37**, 653 (2004).
[15] Y. M. Qiao and S. Chandra, Experiments on adding a surfactant to water drops boiling on a hot surface, Proc. R. Soc. London Ser. A **453**, 673 (1997).
[16] C. M. Weickgenannt, Y. Zhang, S. Sinha-Ray, I. V. Roisman, T. Gambaryan-Roisman, C. Tropea, and A. L. Yarin, Inverse-Leidenfrost phenomenon on nanofiber mats on hot surfaces, Phys. Rev. E **84**, 036310 (2011).
[17] J. D. Bernardin, C. J. Stebbins, and I. Mudawar, Mapping of impact and heat transfer regimes of water drops impinging on a polished surface, Int. J. Heat Mass Transfer **40**, 247 (1997).
[18] G. Castanet, T. Lienart, and F. Lemoine, Dynamics and temperature of droplets impacting onto a heated wall, Int. J. Heat Mass Transfer **52**, 670 (2009).
[19] A.-B. Wang, C.-H. Lin, and C.-C. Chen, The critical temperature of dry impact for tiny droplet impinging on a heated surface, Phys. Fluids **12**, 1622 (2000).
[20] V. Bertola, An impact regime map for water drops impacting on heated surfaces, Int. J. Heat Mass Transfer **85**, 430 (2015).
[21] A. L. N. Moreira, A. S. Moita, E. Cossali, M. Marengo, and M. Santini, Secondary atomization of water and isooctane drops impinging on tilted heated surfaces, Exp. Fluids **43**, 297 (2007).
[22] G. E. Cossali, M. Marengo, and M. Santini, Thermally induced secondary drop atomisation by single drop impact onto heated surfaces, Int. J. Heat Fluid Flow **29**, 167 (2008).
[23] J. Kim, Spray cooling heat transfer: The state of the art, Int. J. Heat Fluid Flow **28**, 753 (2007).
[24] J. Yang, L. C. Chow, and M. R. Pais, Nucleate boiling heat transfer in spray cooling, ASME J. Heat Transfer **118**, 668 (1996).
[25] D. P. Rini, R.-H. Chen, and L. C. Chow, Bubble behavior and nucleate boiling heat transfer in saturated FC-72 spray cooling, ASME J. Heat Transfer **124**, 63 (2002).
[26] J. Wendelstorf, K-H. Spitzer, and R. Wendelstorf, Spray water cooling heat transfer at high temperatures and liquid mass fluxes, Int. J. Heat Mass Transfer **51**, 4902 (2008).
[27] E. A. Silk, J. Kim, and K. Kiger, Spray cooling of enhanced surfaces: Impact of structured surface geometry and spray axis inclination, Int. J. Heat Mass Transfer **49**, 4910 (2006).
[28] C. Sodtke and P. Stephan, Spray cooling on micro structured surfaces, Int. J. Heat Mass Transfer **50**, 4089 (2007).
[29] L. Lin and R. Ponnappan, Heat transfer characteristics of spray cooling in a closed loop, Int. J. Heat Mass Transfer **46**, 3737 (2003).
[30] K. A. Estes and I. Mudawar, Correlation of sauter mean diameter and critical heat flux for spray cooling of small surfaces, Int. J. Heat Mass Transfer **38**, 2985 (1995).

[31] V. S. J. Craig, B. W. Ninham, and R. M. Pashley, Effect of electrolytes on bubble coalescence, Nature (London) **364**, 317 (1993).
[32] Q. Cui, S. Chandra, and S. McCahan, The effect of dissolving salts in water sprays used for quenching a hot surface: Part 1—Boiling of single droplets, ASME J. Heat Transfer **125**, 326 (2003).
[33] G. Keitel and U. Onken, Inhibition of bubble coalescence by solutes in air/water dispersions, Chem. Eng. Sci. **37**, 1635 (1982).
[34] G. Marrucci, A theory of coalescence, Chem. Eng. Sci. **24**, 975 (1969).
[35] See Supplemental Material at http://link.aps.org/supplemental/10.1103/PhysRevFluids.2.074301 for videos of the bottom and side view of the drop impact and evaporation in the nucleate boiling regime shown in Figs. 4 and 6.
[36] S. G. Bankoff, Entrapment of gas in the spreading of a liquid over a rough surface, AIChE J. **4**, 24 (1958).
[37] V. Mehdi-Nejad, J. Mostaghimi, and S. Chandra, Air bubble entrapment under an impacting droplet, Phys. Fluids **15**, 173 (2003).
[38] S. T. Thoroddsen, T. G. Etoh, K. Takehara, N. Ootsuka, and Y. Hatsuki, The air bubble entrapped under a drop impacting on a solid surface, J. Fluid Mech. **545**, 203 (2005).
[39] M. Schremb, I. V Roisman, and C. Tropea, Transient effects in ice nucleation of a water drop impacting onto a cold substrate, Phys. Rev. E. **95**, 022805 (2017).
[40] W. M. Rohsenow, A method of correlating heat transfer data for surface boiling of liquids, J. Heat Transf.-Trans. ASME **74**, 969 (1952).
[41] H. K. Forster and N. Zuber, Dynamics of vapor bubbles and boiling heat transfer, AIChE J. **1**, 531 (1955).
[42] J. D Bernardin and I. Mudawar, A Leidenfrost point model for impinging droplets and sprays, J. Heat Transf.-Trans. ASME **126**, 272 (2004).
[43] J. D. Bernardin and I. Mudawar, A cavity activation and bubble growth model of the Leidenfrost point, ASME J. Heat Transfer **124**, 864 (2002).
[44] V. P Carey, *Liquid-Vapor Phase-Change Phenomena* (Hemisphere, New York, 1992).
[45] I. V. Roisman, Fast forced liquid film spreading on a substrate: Flow, heat transfer and phase transition, J. Fluid Mech. **656**, 189 (2010).
[46] G. E. Myers, *Analytical Methods in Conduction Heat Transfer* (Genium Publishing Corporation, Schenectady, NY, 1987).
[47] M. Schremb, S. Borchert, E. Berberovic, S. Jakirlic, I. V Roisman, and C. Tropea, Computational modeling of flow and conjugate heat transfer of a drop impacting onto a cold wall, Int. J. Heat Mass Transfer **109**, 971 (2017).
[48] H. K. Forster and N. Zuber, Growth of a vapor bubble in a superheated liquid, J. Appl. Phys. **25**, 474 (1954).
[49] P. Griffith, Bubble growth rates in boiling, J. Heat Transf.-Trans. ASME **80**, 721 (1958).
[50] B. B. Mikic and W. M. Rohsenow, Bubble growth rates in non-uniform temperature field, Prog. Heat Mass Transfer **2**, 283 (1969).
[51] L. D. Landau and B. G. Levich, Dragging of a liquid by a moving plate, Acta Physicochim. U.R.S.S. **17**, 42 (1942).
[52] S. J. D. Van Stralen, M. S. Sohal, R. Cole, and W. M. Sluyter, Bubble growth rates in pure and binary systems: Combined effect of relaxation and evaporation microlayers, Int. J. Heat Mass Transfer **18**, 453 (1975).
[53] P. Stephan and J. Hammer, A new model for nucleate boiling heat transfer, Heat Mass Transfer **30**, 119 (1994).
[54] M. Abu-Zaid, An experimental study of the evaporation characteristics of emulsified liquid droplets, Heat Mass Transfer **40**, 737 (2004).
[55] I. Buchmüller, Influence of pressure on Leidenfrost effect, Ph.D. thesis, TU Darmstadt, Darmstadt 2014.
[56] M. Itaru and M. Kunihide, Heat transfer characteristics of evaporation of a liquid droplet on heated surfaces, Int. J. Heat Mass Transfer **21**, 605 (1978).
[57] P. Tartarini, G. Lorenzini, and M. R. Randi, Experimental study of water droplet boiling on hot, non-porous surfaces, Heat Mass Transfer **34**, 437 (1999).

[58] A. Faghri and Y. Zhang, *Transport Phenomena in Multiphase Systems* (Academic Press, San Diego, 2006).
[59] N. Siemons, H. Bruining, H. Castelijns, and K.-H. Wolf, Pressure dependence of the contact angle in a CO2-H2O–coal system, J. Colloid Interface Sci. **297**, 755 (2006).
[60] S.-S. Hsieh, T.-C. Fan, and H.-H. Tsai, Spray cooling characteristics of water and R-134a. Part I: Nucleate boiling, Int. J. Heat Mass Transfer **47**, 5703 (2004).